RSC Advances

ROYAL SOCIETY OF CHEMISTRY

www.rsc.org/advances

ARTICLE TYPE www. rsc.org/xxxxxx | XXXXXXXX

Electronic and Charge Transport Properties of Dimers of Dithienothiophenes: Effect of Structural Symmetry and Linking Mode

Ping Li, Yahui Cui, Chongping Song and Houyu Zhang*

Received Xth XXXXXXXXXX 20XX, Accepted Xth XXXXXXXXX 20XX
First published on the web Xth XXXXXXXXXX 200X
DOI: 10.1039/b000000x

The electronic structures and charge transport properties of a series of dimers of dithienothiophenes are investigated by means of quantum chemical calculations. To gain a better understanding of the effects of the structural symmetry and linking mode on dimers, the geometrical structures, molecular reorganization energies upon getting or losing electrons, molecular ionization potentials (IPs) and electron affinities (EAs), molecular aromaticities, frontier molecular orbitals, as well as charge mobilities are analyzed in detail to determine the structure-property relationships for the investigated dimers of dithienothiophenes. The calculated results show that the vinylene-linked dimers have the advantages over the directly single-bond linked dimers because of the large extent of π conjugation and thus enhanced $\pi-\pi$ stacking interactions in their crystal structures. The molecular symmetry could affect the electron density distributions in the molecules, and further determine the molecular orientations and intermolecular arrangements. The high molecular symmetry could facilitate the molecular packing in order, thus enhancing the charge transport. The theoretical characterization of these dimers in combination with experimental results indicate that high symmetrical vinylene-bridged dimers could be promising candidates for transistor applications, and shed light on the molecular design of high performance materials.

Introduction

Organic semiconductors (OSCs) have drawn continuous attention for decades due to their prospective commercialized applications in electronic devices, such as organic field effect transistors (OFETs)[1–7], organic solar cells[8–10], and organic light emitting diodes (OLEDs)[11–13]. Among the most extensively studied OSCs, oligothiophene-based conjugated materials are important representative systems owing to their chemical versatility, favorable electrical and optical properties[14,15]. α-oligothiophenes have been successfully applied as active components in OLEDs and OFETs, but the low conjugation because of the torsion of single bonds or S-syn defects limit their optical and charge-transport performances in practical devices[16]. While the fused oligothiophenes (thienoacenes) possess the advantages of extended conjugation and rigid planarity, thus leading to the improved charge transporting properties and chemical stability[17–19]. The sulfur atoms in thienoacenes have the high polarizability and thus facilitate electron-donating properties. Multiple short intermolecular S$\cdots$S contacts originated from sulfur atoms at the molecular periphery can make the molecules densely packed in the solid state, resulting in the enhanced charge transport properties.

The structures of thienoacenes rely on selective connections and annelations of thiophene building blocks at α-, and β-positions, which will lead to quasi-linearly annelated α-thienoacenes and helically annelated β-thienoacenes[20]. The oligothienoacenes of dithieno[3,2-b:2′,3′-d]-thiophene and dithieno[2,3-b:3′,2′-d]-thiophene (hereafter denote as α- and β-trithiophene) are regarded as effective molecular building units with quite different LUMO character and HOMO-LUMO gaps (as shown in Fig. 1a), and can be used to design the versatile OSCs. The dimerizations of α- and β-trithiophenes linked by single bond (**1**-**3**) and vinylene bridge (**4**-**6**) were constructed as new candidates for OFET materials (Fig. 1b)[21]. The dimer of α-trithiophene **1** has been demonstrated to be effective as the active layer in FET device and shows hole mobility of up to 0.05 $cm^2V^{-1}s^{-1}$ [22,23]. The mobility of the dimer of β-trithiophene **2** is 0.005 $cm^2V^{-1}s^{-1}$ at the room temperature, while the device performance of vinylene-bridged dimer of β-trithiophene **5** is apparently much better than that of **2**, exhibiting excellent OFET performance with mobility as high as 0.89 $cm^2V^{-1}s^{-1}$ [24]. The questions on why the subtle structural changes lead to significant effect on the charge transport properties should be revealed in microscopic level and a detailed understanding of the structure-property relationship should be established for these OSCs.

In present work, we focus on the effects of structural symmetry and linking mode on the electronic structures of the dimers of dithienoacenes. The compounds **1**, **2**, **4** and **5** ar

State key laboratory of supramolecular structure and materials, Institute of theoretical chemistry, Jilin university, Changchun 130012, P.R. China, Tel: 86-431-85168492; E-mail: houyuzhang@jlu.edu.cn

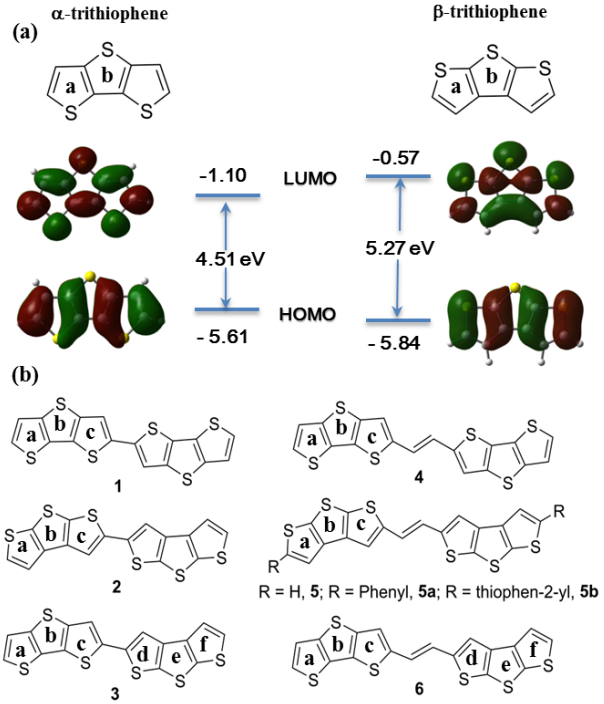

Fig. 1 (a) The chemical structures of α- and β-trithiophenes with their frontier orbitals and HOMO-LUMO gaps and (b) the dimer structures investigated in this work. The letters denote symmetry-unique rings in these molecules.

highly symmetrical in structure, while the cross-linked compounds **3** and **6** are asymmetrical. How and to what extent the structural symmetry affect the intermolecular interactions of these thienoacenes need to be elucidated. The question on why the different linking modes linked by either directly single bond or vinylene bridge could result in distinct electronic properties still need to be answered. The molecular geometries, the molecular frontier orbitals, molecular IPs and EAs, and reorganization energies will be definitely influenced by the structural symmetry and linking mode in the dimerization of dithienoacenes. Additionally, the α- and β-trithiophenes have different π-conjugation and exhibit distinct aromaticity originated from the location of sulfur atoms in the molecular backbone. The aromaticity in the dimer structure will subtly change in comparison to that of their monomer counterpart. All these electronic properties need to be investigated to further understand the relationship with the structural changes at a microscopic level.

Theoretical calculation is becoming a powerful tool to study the electronic properties of OSCs and predict their charge transport properties[25–32]. At a high-temperature regime and in the presence of structural disorders, charge carriers are localized over a single molecule,[33,34] which make the bandlike mechanism fail in describing the transport behavior in many OSCs[35,36]. Thus, a thermally activated hopping and diffusion model can be employed to simulate the charge carrier motion[37–39]. Based on quantum-chemical calculations, we make comparative studies of the electronic and charge transport properties of the dimers of α- and β-trithiophene. By means of density functional theory (DFT) calculations, we aim to establish structure-property relationships of thienoacenes-based materials and shed light on the fundamental research on designing high charge mobility materials.

Theoretical and computational method

The molecular geometries of neutral and charged states are optimized at the DFT level using B3LYP hybrid functional[40,41] and 6-31G(d, p) basis set, as implemented in the Gaussian 0[illegible] package[42]. Harmonic vibrational frequencies are calculated at the same level of theory on the basis of resulting optimized geometries. The total density of state (DOS) and projected density of state (PDOS) for sulfur atom and phenyl (or thienyl) group are obtained with GaussSum 2.25 program[43].

To study the charge transport properties of the dimers of dithienothiophenes at room temperature, the incoherent hopping mechanism is adopted to describe the sequential charge jumps between adjacent molecules. For each charge hopping event, the self-exchange charge transfer rate can be expressed by the Marcus-Hush equation[44,45] in terms of reorganization energy λ and electronic coupling V_{ab} between neighboring molecules a and b[46]:

$$k = \frac{2\pi V_{ab}^2}{h}\left(\frac{\pi}{\lambda k_B T}\right)^{1/2}\exp\left(-\frac{\lambda}{4k_B T}\right) \quad (1)$$

where, T is room temperature (298K), and k_B is the Boltzmann constant. Assuming no correlation between charge hopping events and charge motion is a homogeneous random walk[26], the drift mobility, μ, is related to the diffusion coefficient D and charge transfer rate k as:

$$\mu = \frac{e}{k_B T}D; D = \frac{1}{2n}\sum_i d_i^2 k_i P_i \quad (2)$$

where e is the electronic charge. Considering the charge motion as a random walk in three dimensions (n = 3), D is summation over all possible hops. P_i is the probability ($P_i = k_i/\sum k_i$) for charge transfer to ith neighbor and d_i is the intermolecular center-to-center distance. The reorganization energy λ consists of contributions from the inner reorganization energy (which is induced by intramolecular vibrations) and the external reorganization energy[47] (which is caused by polarization of the surrounding medium). For organic solids and weak polar media, the contribution to the reorganization energy from electronic polarization of surrounding molecules i

quite small and on the order of a few tenths of an electronvolt, so the external reorganization energy can be neglected[48,49]. Herein, only the intramolecular reorganization energy is calculated directly from the relevant points on the adiabatic potential energy surfaces (PES) using the standard procedure detailed in the literature[38,50,51]. The transfer integral V_{ab} characterizes the degree of molecular orbital overlapping between two adjacent molecules. Here, we take the single crystal structure to generate all possible intermolecular hopping pathways. The couplings between all these dimers are calculated through a direct approach using Fock operator[52–54]:

$$V_{ab} = \langle \Psi_i^{0,a} | F^0 | \Psi_i^{0,b} \rangle \quad (3)$$

where $\Psi_i^{0,a}$ and $\Psi_i^{0,b}$ represent the molecular frontier orbitals of isolated molecules a and b, where i denote the highest occupied molecular orbitals (HOMO) for hole transfer and lowest unoccupied molecular orbitals (LUMO) for electron transfer. F^0 is the Fock operator for the dimer in a specific pathway, the superscript zero indicates that the molecular orbitals appearing in the operator are unperturbed. The Fock matrix can be evaluated by $F = SC\varepsilon C^{-1}$, with S is the intermolecular overlap matrix, and C and ε are the molecular orbital coefficients and eigenvalues, respectively.

The choice of DFT functional is important for an accurate description of the ground-state electronic properties and electronic couplings between adjacent molecules. In comparison to pure DFT functionals, hybrid functionals can give a better estimate of HOMO-LUMO energy gap because of the incorporation of a fraction of non-local Hartree-Fock (HF) exchange. While long-range corrected functionals are better than hybrid functionals in describing the charge-transfer excited state in push-pull molecules.[55,56] In this work, the electronic coupling is calculated from the overlap of the ground-state frontier orbtials of adjacent molecules. Such calculations do not involve the excited charge transfer. So hybrid functionals such as B3LYP[57,58], M062X[59], and MPWB1K[31] and combined exchange-correlation functional PW91PW91[29,33,60] are used to calculate the electronic couplings in the literatures. Hence hybrid functional B3LYP is employed to calculate the ground-state electronic structures and electronic couplings in the dimer structures.

The analyses of the local aromaticity in all compounds are performed by means of nucleus independent chemical shifts (NICS(1)), and harmonic oscillator model of aromaticity (HOMA) index. The calculated NICS(1) and HOMA values provide a relative comparison of aromaticity among all of the compounds. In the NICS(1) procedure suggested by Schleyer *et al.*[61], the absolute magnetic shielding is computed at 1 Å above and 1 Å below the center of the ring (for the heterocyclic ring in this work, we define the center as the ring

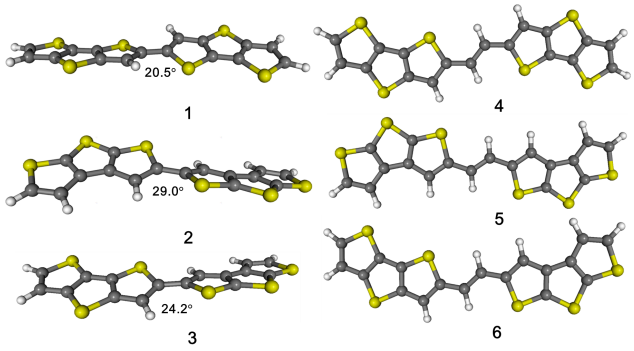

Fig. 2 Optimized structures in the neutral state of the investigated molecules.

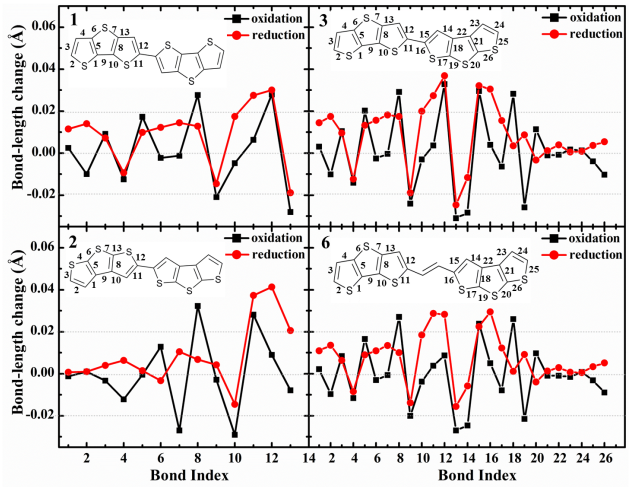

Fig. 3 Bond-length changes (in Å) upon oxidation and reduction for compounds **1**, **2**, **3** and **6**. The bond indices are labelled on the molecular structures.

bonding critical point). The HOMA index is calculated as

$$\mathrm{HOMA} = 1 - \frac{1}{n}\sum_i^n \alpha(R_{\mathrm{opt}} - R_i)^2 \quad (4)$$

where n is the number of bonds of the ring considered, α is a normalization constant, R_{opt} is the optimal bond length for a fully delocalized π-electron system, and R_i stands for an actual bond length. In the present work, we used the parameters needed for the HOMA calculations proposed by Krygowski[62]: $\alpha_{\mathrm{CC}} = 257.7$, $\alpha_{\mathrm{CS}} = 94.09$, $R_{\mathrm{opt}}^{\mathrm{CC}} = 1.388$, and $R_{\mathrm{opt}}^{\mathrm{CS}} = 1.677$.

Results and disscussion

Molecular geometry and reorganization energy

The optimized structures of the investigated molecules in the neutral state for the gas phase are shown in Fig. 2. Thoug

Table 1 Internal reorganization energies for hole and electron (λ_h and λ_e), ionization potentials (IPs) and electron affinities (EAs) of adiabatic/vertical (A/V) calculated with basis set of 6-31G++(d, p) and 6-31G(d, p) (in parentheses) in the unit of eV.

compd.	λ_h	λ_e	AIP	VIP	AEA	VEA
1	0.338 (0.332)	0.298 (0.295)	6.42 (6.23)	6.60 (6.41)	-1.08 (-0.77)	-0.91 (-0.60)
2	0.381 (0.373)	0.358 (0.380)	6.67 (6.50)	6.89 (6.71)	-0.58 (-0.20)	-0.36 (0.02)
3	0.359 (0.350)	0.326 (0.326)	6.53 (6.35)	6.74 (6.55)	-0.86 (-0.53)	-0.67 (-0.34)
4	0.292 (0.298)	0.245 (0.255)	6.21 (6.02)	6.36 (6.17)	-1.32 (-1.01)	-1.19 (-0.89)
5	0.308 (0.302)	0.274 (0.293)	6.41 (6.24)	6.56 (6.39)	-0.93 (-0.60)	-0.80 (-0.46)
5a	0.307 (0.311)	0.255 (0.252)	6.33 (6.15)	6.48 (6.30)	-1.03 (-0.72)	-0.91 (-0.59)
5b	0.290 (0.286)	0.209 (0.209)	6.36 (6.18)	6.50 (6.31)	-1.08 (-0.78)	-0.98 (-0.67)
6	0.298 (0.304)	0.259 (0.272)	6.31 (6.12)	6.46 (6.27)	-1.15 (-0.83)	-1.02 (-0.70)

α- and β-trithiophene exhibit the planar and rigid skeleton, the dimers linked by a single bond render twisted structures with dihedral angles about 20.5°, 29.0° and 24.2° for **1**, **2** and **3**, respectively. The dihedral angle between the two triphiophenes in **1** is similar to that value between two thiophenes in α-bithiophene (22°). The compound **2** and **3** show more distorted structures, while the dimers bridged by vinylene show planar structures. The dimer **1** and **2** have C_2 symmetry, while **4** and **5** have C_{2h} symmetry due to the planarity. The cross-linked dimer **3** and **6** have no symmetries in structures. When a molecule gains or loses charges, it will relax its molecular geometry for a new charge distribution. All the cationic and anionic state for the compound **1**-**6** are almost planar structures. The changes of bond lengths upon oxidation (losing electron from the neutral to the cationic state) and reduction (gaining electron from the neutral to the anionic state) of **1**, **2**, **3** and **6** are presented in Fig. 3. Because of the extended π-system, the changes of bond lengths upon oxidation and reduction are founded to occur over the entire molecule, especially more pronounced in the thiophene rings at the linkage. For the asymmetric cross-linked **3** and **6**, the bond length changes in the α-triphiophene are more notable than those in β-trithiophene. The bond length changes of **3** are a bit larger than those of **6** because of the distorted geometrical relaxation from non-planarity to planarity. The bond length changes upon oxidation and reduction are comparable for the selected compounds. Gaining or losing charges causes the changes in geometrical structure, which is a reflection of the reorganization energy.

From the Equation 1, we know that the charge hopping rate benefits from smaller reorganization energy. The reorganization energies of the investigated compounds are collected in Table 1. Compound **2** have the largest reorganization energies for both hole and electron, which is in agreement with the larger bond-length changes in Fig. 3. The reorganization energies of the dimers of α-trithiophenes are smaller than those of the counterpart dimers of β-trithiophenes, while the reorganization energies of the cross-linked dimers (**3** and **6**) are in between the dimers of α- and β-trithiophene. The reorganization energies are to a large extent dependent on the intrinsic properties of α- and β-fused trithiophenes. The reorganization energies for both electron and hole of vinylene-bridged dimers (**4**, **5**, and **6**) are smaller than their corresponding counterpart (**1**, **2**, and **3**) of single-bond linked dimers. The vinylene bridge can significantly decrease the steric hindrance between trithiophene units at the linkage and extend π conjugation, resulting in more rigid and planar structures with higher molecular symmetries. All the molecules have relatively smaller electron reorganization energies because of existence of high polarizability of sulfur atom. As for the introduction of the substituted benzene and thiophene units at the longitudinal ends of **5**, the reorganization energies are reduced, especially for the electron reorganization energy in **5b**.

Molecular IP and EA

The efficient injections of holes and electrons are important for the rational design of optimized electronic devices. The molecular IP and EA are key parameters to estimate the energy barrier for injection of hole and electron into molecule and provide useful information regarding ambient stability.[63] The calculated IPs and EAs of compounds for both adiabatic (optimized structure for both the neutral and charged molecules) and vertical (at the geometry of the neutral molecule) values are presented in Table 1. Since the IPs and EAs are very dependent on the diffuse function of basis set,[64] the calculated results are performed with the large basis set of 6-31++G(d,p) in comparison with 6-31G(d,p). The energy difference between adiabatic and vertical value could reflect the extent of the structural relaxation upon charge injection.[65] The calculated adiabatic and vertical IPs are larger than the adiabatic experimental IP for a stable *p*-type OFET material sexthiophene (5.80 eV)[66], indicating that all the compounds are more stable and exhibit the antioxidative ability in air. Upon going from the single-bond linked dimers to the vinylene-bridged dimers, the adiabatic IPs decrease slightly by 0.2∼0.4 eV, but the compounds are still stable and in favor of reducing th

hole-injection barrier for the commonly used electrode (Au work function: ∼5.1 eV).

In addition to the decrease in IPs, the vinylene bridge also makes the EAs of dimers more exothermic. The negative value of EA indicates exothermicity for the reduction of a molecule, for example, **5** is 0.35 eV more exothermic than **2**. The vinylene-bridged dimers have small EA values ranged from -0.93 eV to -1.32 eV (see Table 1 for the adiabatic value of EAs). The calculated EA values are not matchable to the workfunction of the commonly used metallic electrodes (∼3 eV) and less stable upon reduction. We can see that vinylene-bridged dimers have more negative EAs, which are of great benefit to lowering the energy barrier for electron injection and improving the stability of their anions by preventing chemical reactions with water and oxygen.

From the redox stability point of view, the single-bond linked dimers are more stable in their cationic states and less stable in their anion states than their conresponding counterpart of vinylene-bridged dimers. In comparison to α-trithiophene dimers, β-trithiophene dimers have larger IPs and EAs. The cross-linked dimers have the IPs and EAs in between dimers of α- and β-trithiophene. This change trend is in well agreement with that of reorganization energy. It is noticeable that the introduction of phenyl or thienyl group at the longitudinal ends of **5** decrease both IPs and EAs, which are further favorable for improving hole or electron injection.

Structure and aromaticity

Aromaticity is the property of a planar, cyclic, conjugated molecule in which cyclic electron delocalization results in enhanced stability, bond length equalization, and special magnetic, chemical and physical properties[67,68]. The α- and β-trithiophenes are aromatic because the molecules are cyclic and planar structures, and follow Huckel's rule, having $4n$+2 electrons in the delocalized π-orbitals. The aromatic properties will slightly change when two trithiophene subunits are linked through a single bond or a vinylene bridge. Considering the fact that the molecular geometry determined by the extent of π-conjugation is an important factor to determine the electronic structures of dimers, we evaluate the aromaticity of the heterocyclic rings of the dimers for understanding the molecular structure-property relationship.

The calculated NICS(1) and HOMA values are collected in Table 2. For the building block α- and β-trithiophenes, the absolute values of NICS(1) and HOMA of central rings (***b***) are smaller than those of the periphery rings (***a***), as indicated in Fig. 1b. The average absolute values of NICS(1) and HOMA for all aromatic rings in α-trithiophenes are larger than that in β-trithiophenes, which indicates that electrons are more delocalized in α-trithiophenes. α-trithiophene has larger extent of π-conjugation than β-trithiophene, which is in agreement with the smaller HOMO-LUMO gap in α-trithiophene (as shown in Fig. 1a). The aromaticity differences between α- and β-trithiophene originate from the location of sulfur atoms in the molecular backbone, as can be seen from their LUMO character in Fig. 1a. While in the dimer structures, the absolute values of NICS(1) and HOMA of the rings at the linkage dramatically decrease, resulting in the average aromaticity decrease in both single-bond and vinylene-bridge linked dimers. The average aromaticity in the vinylene-brdiged dimers is smaller than that of the single-bonded dimers. In previous report, Chen *et al.* studied the relationship between aromaticity and conductance of a single-molecule junction and verified that the conductanc correlates negatively with the aromaticity[69]. So the decrease of the aromaticity of the compounds might be in favour of charge hopping between the heterocyclic rings.

Table 2 NICS(1) and HOMA values of individual heterocyclic rings for the compounds. The rings a-f are indicated in Fig. 1.

compd.	ring	NICS(1)	NICS(1)[a]	HOMA	HOMA[a]
α	a	-8.624	-8.204	0.726	0.711
	b	-7.365		0.681	
β	a	-8.721	-8.123	0.691	0.669
	b	-6.925		0.624	
1	a	-8.678	-7.718	0.729	0.705
	b	-7.211		0.690	
	c	-7.418		0.696	
2	a	-8.733	-7.670	0.693	0.662
	b	-6.801		0.627	
	c	-7.474		0.665	
3	a	-8.524	-7.774	0.729	0.683
	b	-7.275		0.686	
	c	-7.351		0.697	
	d	-7.316		0.667	
	e	-7.433		0.626	
	f	-8.747		0.694	
4	a	-8.511	-7.623	0.730	0.705
	b	-7.233		0.691	
	c	-7.126		0.694	
5	a	-8.793	-7.610	0.694	0.662
	b	-6.780		0.627	
	c	-7.256		0.664	
6	a	-8.530	-7.612	0.731	0.686
	b	-7.221		0.680	
	c	-7.158		0.716	
	d	-7.248		0.667	
	e	-6.739		0.627	
	f	-8.772		0.695	

[a] The average value for all heterocyclic aromatic rings.

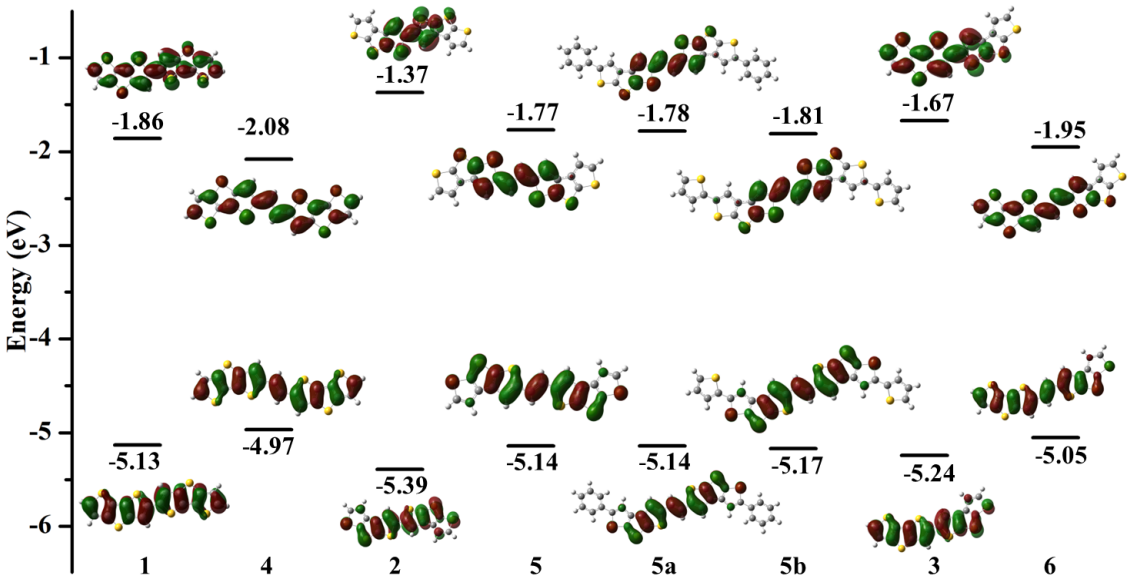

Fig. 4 HOMO and LUMO energy levels of all the studied molecules and their electronic density contours investigated by the B3LYP/6-31G(d, p) method.

Molecular orbital and density of state

Frontier orbitals, especially HOMO and LUMO, are closely related to gain and loss electrons during the charge transport. The relative orderings of HOMO and LUMO energies provide a reasonable qualitative indication of the ability of hole and electron injection, respectively. A good p-type conducting material is required to have a relatively high HOMO for reducing the charge injection barrier from anode. The HOMO and LUMO plots and orbital energy levels of the dimers are displayed in Fig. 4, and their experimental values are listed in Table 3. It shows that the calculated HOMO and LUMO energies are in agreement with the experimentally measured values, especially with a change in trend.[70] The dimers of α- and β-trithiophene (**1** and **2**) possess higher HOMOs, lower LUMOs and smaller HOMO-LUMO gaps than their monomers (as shown in Fig. 1a). The vinylene-bridged dimers (**4**, **5** and **6**) also have the higher HOMOs, lower LUMOs and smaller HOMO-LUMO gaps with respect to their corresponding single-bond linked dimers (**1**, **2** and **3**). Such observations can be attributed to the extension of π-conjugation. Both raising HOMOs and lowering LUMOs are in favor of charge injections in practical application in devices. In the dimers of α-trithiophene (**1** and **4**), the HOMO and LUMO spread over the entire molecules. While the HOMO and LUMO are concentrated on the central part of the dimers of β-trithiophenes. Both dimers of α- and β-trithiophene have symmetric HOMOs and LUMOs distribution in the structures, while the dimers of cross-linked α- and β-trithiophene have asymmetrical distribution of frontier orbitals, with the HOMO and LUMO located more on α-trithiophenes than those on β-trithiophenes.

Table 3 HOMO and LUMO energy levels and their gaps calculated at the B3LYP/6-31G (d, p) level, together with experimental results.

Compd.	HOMO (eV)		LUMO (eV)	H-L gap	
	Theo.	Expt.[a]	Theo.	Theo.	Expt.[a]
1	-5.13	-5.43	-1.86	3.27	2.80
2	-5.39	-5.49	-1.37	4.02	3.15
3	-5.24	-5.46	-1.67	3.57	2.93
4	-4.97	-5.33	-2.08	2.89	2.65
5	-5.14	-5.39	-1.77	3.37	2.91
5a	-5.14	-5.41	-1.78	3.36	2.90
5b	-5.17	-5.42	-1.81	3.36	2.89
6	-5.04	-5.36	-1.95	3.10	2.76

[a] Data from Ref. 20.

The introduction of phenyl and thienyl group at the longitudinal ends of **5** will definitely affect the frontier orbitals of the dimer of vinylene-bridged β-trithiophene. To investigate the substituent effect on the composition of orbitals near the HOMO-LUMO gap, we calculate total DOS and PDOS for three β-annulated oligothiophenes, as shown in Fig. 5. W find that the sulfur atoms partially take part in the formation of both HOMOs and LUMOs. From the electronic structure point of view, the sulfur atoms directly involve the charge car

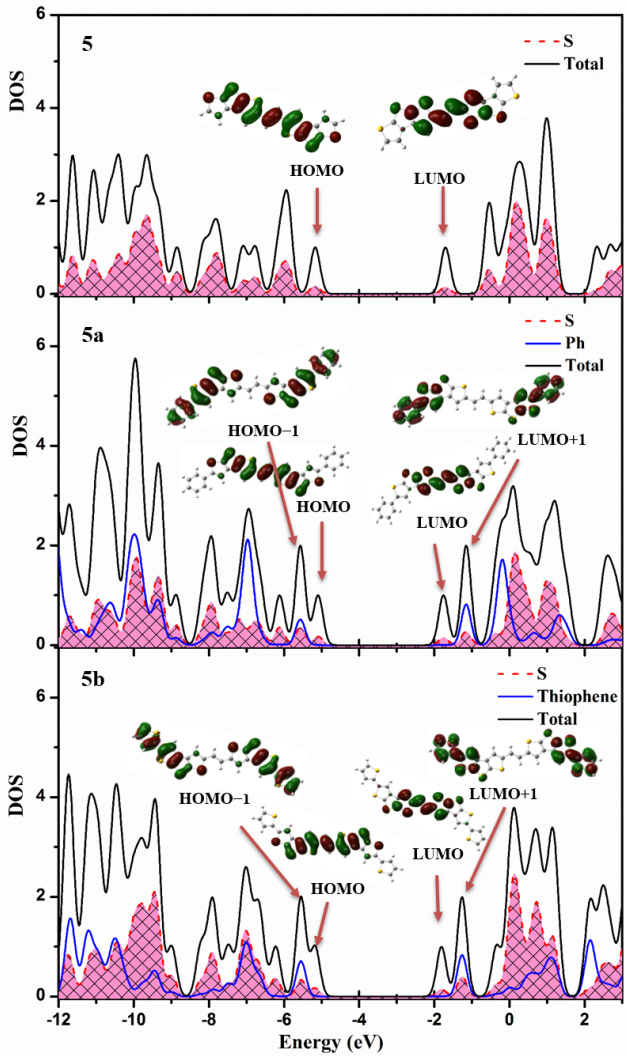

Fig. 5 Total DOS and PDOS for sulfur atom, phenyl and thienyl group in the energy window of -12 and 3 eV for **5**, **5a** and **5b**.

rier transport. Both the HOMOs and LUMOs in **5a** and **5b** are localized in the central part of the compounds. The phenyl and thienyl group do not involve in the formation of HOMOs and LUMOs, but they largely participate in the HOMO-1 and LUMO+1. Because of the existence of dihedral angles between phenyl group or thienyl group and the central π systems about 29.2° and 25.2° respectively, the substituted phenyl or thienyl group can not extend the conjugation of π system largely and only partly involve in the charge transport. From the molecular structure point of view, the phenyl or thienyl group will affect the intermolecular arrangements and orbital interactions, resulting in the different electronic couplings for hole and electron.

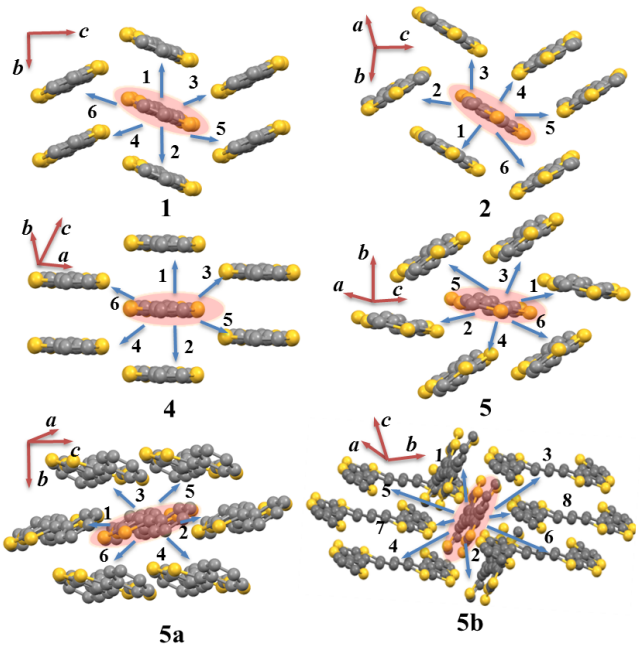

Fig. 6 Charge hopping pathways for compounds **1**, **2**, **4**, **5**, **5a** and **5b**.

Electronic coupling and mobility

The charge transport ability of organic semiconductor is dependent on not only the electronic properties of the molecule itself but also the molecular packing structures. Besides the intrinsic molecular reorganization energy and ability of gaining or losing electron of a molecule, charge transport is highly sensitive to the relative orientations and moleular stacking characters between molecules.[71] The structure of the single crystal could provide a consistent platform to study the structural effects. Therefore, the charge transport properties of oligothiophenes are analyzed on the basis of single crystal structures to reach a deeper understanding of the influence of the structural symmetry and linking mode on the nature of the charge transport.

The experimental results have proved that the two asymmentric molecules **3** and **6** exhibit low mobilities on the order of 10^{-4} $cm^2V^{-1}s^{-1}$ [21]. The likely explanation might be the asymmetric structure induced strong disorder in molecular packing in the amorphous films. From the frontier orbitals standpoint of view, the electron densities are nonuniformly and asymmetrically distributed in α- and β-trithiophenes, as can be seen from the HOMOs and LUMOs of **3** and **6** in Fig. 4. Such electron density distributions are not in favor o the π-orbital interactions, thus affecting the charge transport between the adjacent molecules. The single crystals are not available for asymmetrical **3** and **6** in the experiment becaus

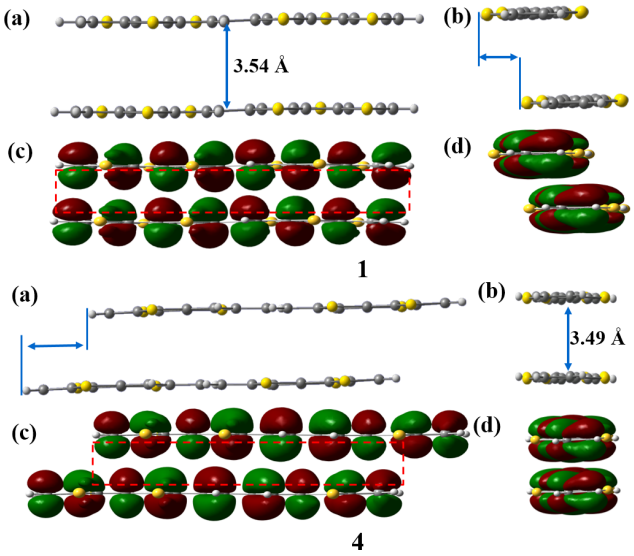

Fig. 7 The dimer geometries and pictorial HOMO interactions of π-π stacking configurations in **1** and **4** viewed along the long molecular axis ((a) and (c)) and the short molecular axis((b) and (d)), respectively.

of structural disorder and lacking of intermolecular π-orbitals interactions. While symmetric molecules **1**, **2**, **4** and **5** are well packed in their crystal structures. It is established that the better the molecular organization in order, the higher the material performance[7]. So the molecular symmetry affect the intermolecular interactions, thus determining the molecular packing structures in their solid states.

The available crystal structures of symmetric compounds are shown in Fig. 6, in which molecules in the same layer in crystal are viewed from the molecular long axis. Choose one molecule as charge donor, and all the surrounding nearest neighbor molecules can be regarded as charge acceptors. The possible intermolecular hopping pathways from central molecule are also displayed in Fig. 6, and the corresponding intermolecular electronic couplings are collected in Table 4. The crystal structures of the dimers of α-trithiophene **1** and **4** have the displaced π-π stacking features with the respective interplanar distances of 3.54 Å and 3.49 Å. The displaced π-stacking configurations and pictorial orbital interactions between HOMOs are displayed in Fig. 7. The π-π stackings in crytals **1** and **4** prefer the slipped configurations because of the existence of strong π-orbital repulsions when molecules are on top of each other. The intermolecular displaced π-π stackings for **1** and **4** are quite different: compound **1** prefers slipping along the molecular short axis about one third of thiophene ring; while compound **4** is shifted in the direction of molecular long axis about three fourths of thiophene ring. The π-π stacking could provide large overlap of π orbital, which is in favor of charge transfer. The electronic couplings for hole of

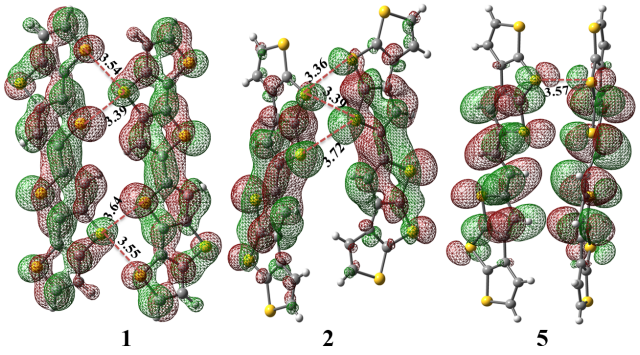

Fig. 8 The pictorial LUMO interactions for short S···S contacts for **1**, **2**, and **5**.

intermolecular π-π stacking interactions of **1** and **4** are 142.2 and 19.6 meV, respectively. From the orbital interactions depicted in Fig. 7, we can rationalize the electronic couplings between the HOMOs. The π-orbitals in **1** are head-to-head interactions, resulting in the enhanced coupling by the overlap of orbital. While the π-orbitals in **2** are mismatched, leading to the noneffective orbital overlap or partial cancelation between the wavefuction of π-orbitals.

The crystal structures of the dimers of β-trithiophene **2** and **5** exhibit the respective sandwich-herringbone and herringbone arrangement. There is a π-stacking pathway in **2** which gives the maximum electronic coupling for hole of 57.8 meV, which is in consistent with previous calculated results (62.2 meV)[24,58]. For compound **5**, the calculated electronic couplings for hole for two kinds of pathways are 15.5 and 33.0 meV respectively. The introduction of phenyl and thienyl group at the longitudinal ends of compound **5** lead to the distinct molecular stacking in the crystal. The compound **5a** has a herringbone arrangement, which is similar to that of **5**. The existence of strong intermolecular phenyl-phenyl and phenyl-trithiophene interactions rationalize the large electronic couplings of 21.0 and 43.5 meV for hole. The crystal structure of **5b** contains multiple interactions, such as slipped π-π interactions and S···S interactions, however, the electronic couplings are relatively small due to the large intermolecular distances.

From the crystal structure, we notice that the short S···S contacts could make the molecules closely packed in the crystal structure. Furthermore such S···S interactions could effectively facilitate electron transport because of the high polarizability of sulfur atoms. The selected short S···S contacts in compounds **1**, **2**, and **5** and LUMO interactions are shown in Fig. 8. Compound **1** have multiple intensive S···S contacts, which are smaller than the sum of the Van der Waals radiu of S atmos (3.70 Å), leading to strong electronic coupling of 20.5 meV for electron. In compound **2** and **5**, strong S···S interactions (3.36 Å and 3.57 Å) are responsible for their larg

Table 4 Electronic couplings V_{ab} of hole and electron for the different hopping pathways of compounds **1**, **2**, **4**, **5**, **5a** and **5b**.

compd.	pathway	d (Å)	V^h_{ab} (meV)	V^e_{ab} (meV)
1	1, 2	3.88	142.2	44.4
	3, 4, 5, 6	5.88	0.3	20.5
2	1	3.74	57.8 (62.2)[a]	23.1
	2, 5	6.29	19.9 (2.7)	76.1
	3	6.75	2.8 (2.0)	12.4
	4, 6	5.16	3.9 (7.4)	64.4
4	1, 2	4.72	19.6	34.4
	3, 4	6.20	0.1	2.3
	5, 6	7.79	6.4	17.4
5	1,2	5.74	15.5 (11.3)	8.9
	3, 4, 5, 6	4.77	33.0 (35.4)	26.7
5a	1, 2	6.17	21.0	7.8
	3, 4, 5, 6	4.80	43.5	41.6
5b	1, 2	6.03	22.6	3.2
	3, 4	9.41	4.5	2.5
	5, 6	12.25	0.7	1.3
	7, 8	13.22	1.0	2.0

[a] Data in parentheses obtained from Ref. 24 and 58.

electronic couplings of 76.1 and 26.7 meV for electron, respectively. Such S···S interactions could be in favor of electron transport.

It has been proved that the anisotropic transport properties would be prominent because of different molecular arrangements in different directions in the crystal. When the charge transport is dominant within a two-dimensional molecular layer and less efficient between molecular layers, the angular resolution anisotropic mobility within a molecular layer can be predicted by the following formula[66]:

$$\mu_\phi = \frac{e}{2k_BT}\sum_i d_i^2 k_i P_i \cos^2(\theta_i - \phi) \qquad (5)$$

where $P_i\cos^2(\theta_i-\phi)$ is the relative hopping probability of various transport pathways to the specific transistor channel. As exampled in Fig. 9a for **5**, ϕ is the orientation angles of the conducting channel relative to the crystallographic axis c and θ_i are the angles of different pathways relative to the reference axis. $\theta_i-\phi$ is the angles between the different pathways and the conducting channel. The anisotropic mobilities for hole in **5** and **5a** are shown in Fig. 9b. We can see clearly the hole mobilities are varied with the ϕ. The hole mobility has maximum value of respective 0.066 $cm^2V^{-1}s^{-1}$ and 0.045 $cm^2V^{-1}s^{-1}$ for **5a** and **5** with ϕ of 90°. The anisotropic mobilities for the available crystal structures of symmetric compounds in specific layers are collected in Table 5, which give the mobilities range for different directions within a crystal plane.

Table 5 The predicted hole and electron average and anisotropic mobilities μ ($cm^2V^{-1}s^{-1}$), together with the experimental values.

	Theo.		Aniso.		Exp.
	μ_h	μ_e	μ_h	μ_e	μ
1	0.23	0.03	0-0.69	0.013-0.073	0.05[a]
2	0.02	0.08	0.0016-0.061	0.057-0.20	0.005[b]
4	0.0087	0.052	0-0.026	0.013-0.12	0.08[c]
5	0.023	0.018	0.028-0.045	0.020-0.035	0.89[b]
5a	0.039	0.074	0.051-0.066	0.091-0.13	2.0[d]
5b	0.022	0.0086	0-0.068	0-0.026	0.002[e]

[a] Ref. 22 and 23; [b] Ref. 21 and 24; [c] Ref. 21; [d] Ref. 73; [e] Ref. 20.

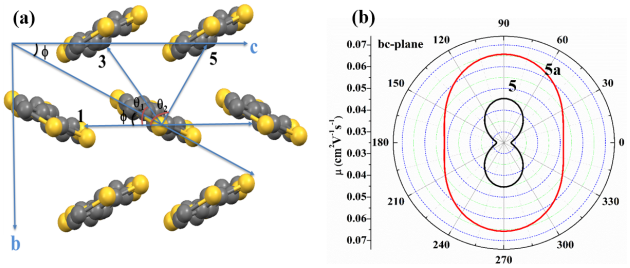

Fig. 9 The angle-dependent hopping paths projecting to a transistor channel in the bc plane (a) and calculated angle-resolved anisotropic hole mobilities (b) of **5** and **5a**, respectively.

The predicted average mobilities are listed in Table 5, together with the available experimental data. The calculated hole mobility of **1** is 10 times of that of **2**, which is well consistent with the experimental values. Compound **1** prefers transporting holes because of relatively smaller reorganization energy and larger electronic couplings for hole. While compound **2** prefers electron transport since the existence of multiple short S···S interaction enhances the electronic couplings for electron. The predicted hole mobilities for **5** and **5a** are slightly larger than that of **2** and much smaller than experimental values. The vinylene bridge in the compound **5** and **5a** decreases the reorganization energy, the hole injection barrier and aromaticity, which could be beneficial to increase the hole mobility. Considering the fact that the experimental mobilities are strongly influenced by the the microstructural characteristics of the dielectric layers in OFETs, such as film deposition temperature, film growth mode, and semiconductor phase composition[72], our calculated mobility based on the crystal structures can be regarded as a reference.

Conclusions

In summary, the electronic and charge transport properties of dimers of dithienothiophenes have been investigated by DFT calculations. The frontier orbitals of the dimers have the same symmetry as the molecular symmetry, indicating that the molecular symmetry determines the the electron density distribution in the molecules. The symmetries of the dimers also influence the molecular arrangements in the crystal states. The vinylene-bridged dimers have relatively smaller reorganization energies, more matchable HOMO and LUMO levels to the electrode of the device, decreased aromaticities and larger mobilities in comparison to single-bond linked dimers. So both the symmetry and linking modes are important to determine the electronic and charge transport properties of dimers of dithienothiophenes.

The calculated results would hint us that the high symmetrical molecule could have advantage in the molecular arrangement in the solid state. The extended π conjugation could enhance the electronic couplings through $\pi - \pi$ stacking interactions, meanwhile, the decreased molecular aromaticity could be more favorable for the charge transport. The high symmetrical vinylene-bridged dimers of dithienothiophenes, or their analogues, could be potential good candidates for transistor applications.

Acknowledgement

We are grateful for the financial support from the National Nature Science Foundation of China (grant nos. 21173101 and 21073077).

References

1 J. E. Anthony, *Chem. Rev.*, 2006, **106**, 5028–5048.
2 V. Coropceanu, J. Cornil, D. A. da Silva Filho, Y. Oliver, R. Silbey and J. L. Bredas, *Chem. Rev.*, 2007, **107**, 926–952.
3 J. Zaumseil and H. Sirringhaus, *Chem. Rev.*, 2007, **107**, 1296–1323.
4 J. E. Anthony, *Angew. chem. int. Ed.*, 2008, **47**, 452–483.
5 Y. Wen, Y. Liu, Y. Guo, G. Yu and W. Hu, *Chem. Rev.*, 2011, **111**, 3358–3406.
6 M. Mas-Torrent and C. Rovira, *Chem. Rev.*, 2011, **111**, 4833–4856.
7 C. Wang, H. Dong, W. Hu, Y. Liu and D. Zhu, *Chem. Rev.*, 2012, **112**, 2208–2267.
8 T. M. Clarke and J. R. Durrant, *Chem. Rev.*, 2010, **110**, 6736–6767.
9 J. E. Allen and C. T. Black, *ACS Nano*, 2011, **5**, 7986–7991.
10 T. Ameri, N. Li and C. J. Brabec, *Energy Environ. Sci.*, 2013, **6**, 2390–2413.
11 S.-C. Lo and P. L. Burn, *Chem. Rev.*, 2007, **107**, 1097–1116.
12 S. Chen, L. Deng, J. Xie, L. Peng, L. Xie, Q. Fan and W. Huang, *Adv. Mater.*, 2010, **22**, 5227–5239.
13 H. Sasabe and J. Kido, *J. Mater. Chem. C*, 2013, **1**, 1699–1707.
14 T. Otsubo, Y. Aso and K. Takimiya, *J. Mater. Chem.*, 2002, **12**, 2565–2575.
15 A. Mishra, C.-Q. Ma and P. Bäuerle, *Chem. Rev.*, 2009, **109**, 1141–1276.
16 X. Zhang, A. P. Côté and A. J. Matzger, *J. Am. Chem. Soc.*, 2005, **127**, 10502–10503.
17 R. M. Osuna, X. Zhang, A. J. Matzger, V. Hernndez and J. T. Lpez Navarrete, *J. Phys. Chem. A.*, 2006, **110**, 5058–5065.
18 X. Zhang, J. P. Johnson, J. W. Kampf and A. J. Matzger, *Chem. Mater.*, 2006, **18**, 3470–3476.
19 Y. M. Sun, Y. Q. Ma, Y. Q. Liu, Y. Y. Lin, Z. Y. Wang, Y. Wang, C. A. Di, K. Xiao, X. M. Chen, W. F. Qiu, B. Zhang, G. Yu, W. P. Hu and D. B. Zhu, *Adv. Funct. Mater.*, 2006, **16**, 426–432.
20 W. Jiang, Y. Li and Z. Wang, *Chem. Soc. Rev.*, 2013, **42**, 6113–6127.
21 L. Zhang, L. Tan, W. Hu and Z. Wang, *J. Mater. Chem.*, 2009, **19**, 8216–8222.
22 H. Sirringhaus, R. H. Friend, X. C. Li, S. C. Moratti, A. B. Holmes and N. Feeder, *Appl. Phys. Lett.*, 1997, **71**, 3871–3873.
23 X.-C. Li, H. Sirringhaus, F. Garnier, A. B. Holmes, S. C. Moratti, N. Feeder, W. Clegg, S. J. Teat and R. H. Friend, *J. Am. Chem. Soc.*, 1998, **120**, 2206–2207.
24 L. Tan, L. Zhang, X. Jiang, X. Yang, L. Wang, Z. Wang, L. Li, W. Hu, Z. Shuai, L. Li and D. Zhu, *Adv. Funct. Mater.*, 2009, **19**, 272–276.
25 M. C. R. Delgado, K. R. Pigg, D. A. da Silva Filho, N. E. Gruhn, Y. Sakamoto, T. Suzuki, R. M. Osuna, J. Casado, V. Hernández, J. T. L. Navarrete, N. G. Martinelli, J. Cornil, R. S. Sánchez-Carrera, V. Coropceanu and J.-L. Brédas, *J. Am. Chem. Soc.*, 2009, **131**, 1502–1512.
26 C. L. Wang, F. H. Wang, Q. K. Li and Z. G. Shuai, *Org. Electron*, 2008, **9**, 635–640.
27 S.-H. Wen, W.-Q. Deng and K.-L. Han, *Phys. Chem. Chem. Phys.*, 2010, **12**, 9267–9275.
28 A. Troisi, *Chem. Soc. Rev.*, 2011, **40**, 2347–2358.
29 H. Li, R. Zheng and Q. Shi, *Phys. Chem. Chem. Phys.*, 2011, **13**, 5642–5650.
30 Y. Geng, J. Wang, S. Wu, H. Li, F. Yu, G. Yang, H. Gao and Z. Su, *J. Mater. Chem.*, 2011, **21**, 134–143.
31 H. Liu, S. Kang and J. Y. Lee, *J. Phys. Chem. B.*, 2011, **115**, 5113–5120.
32 L. Wang, P. Li, B. Xu, H. Zhang and W. Tian, *Org. Electron.*, 2014, **15**, 2476 – 2485.
33 X. D. Yang, L. J. Wang, C. L. Wang, W. Long and S. Z. G., *Chem. Mater.*, 2008, **20**, 3205–3211.
34 X. D. Yang, L. Q. K. and Z. G. Shuai, *Nanotechnology*, 2007, **18**, 424029
35 Y. C. Cheng, R. J. Silbey, D. A. dasilva Filho, C. J. P., C. J. and J. L. Brédas, *J. Chem. Phys.*, 2003, **118**, 3764–3774.
36 A. Troisi and G. Orlandi, *J. Phys. Chem. B.*, 2005, **109**, 1849–1856.
37 K. Sakanoue, M. Motoda, M. Sugimoto and S. Sakaki, *J. Phys. Chem. A.*, 1999, **103**, 5551–5556.
38 J.-L. Brédas, D. Beljonne, V. Coropceanu and J. Cornil, *Chem. Rev.*, 2004, **104**, 4971–5004.
39 W. Q. Deng and W. A. Goddard III, *J. Phys. Chem. B.*, 2004, **108**, 8614–8621.
40 C. T. Lee, W. T. Yang and R. G. Parr, *Phys. Rev. B*, 1988, **37**, 785–789.
41 A. D. Becke, *J. Chem. Phys.*, 1993, **98**, 5648–5652.
42 M. J. Frisch, G. W. Trucks, H. B. Schlegel, G. E. Scuseria, M. A. Robb, J. R. Cheeseman, G. Scalmani, V. Barone, B. Mennucci, G. A. Petersson, H. Nakatsuji, M. Caricato, X. Li, H. P. Hratchian, A. F. Izmaylov, J. Bloino, G. Zheng, J. L. Sonnenberg, M. Hada, M. Ehara, K. Toyota, R. Fukuda, J. Hasegawa, M. Ishida, T. Nakajima, Y. Honda, O. Kitao, H. Nakai, T. Vreven, J. A. Montgomery, Jr., J. E. Peralta, F. Ogliaro, M. Bearpark, J. J. Heyd, E. Brothers, K. N. Kudin, V. N. Staroverov, R. Kobayashi, J. Normand, K. Raghavachari, A. Rendell, J. C. Burant, S. S. Iyengar, J. Tomasi, M. Cossi, N. Rega, J. M. Millam, M. Klene, J. E. Knox, J. B. Cross, V. Bakken, C. Adamo, J. Jaramillo, R. Gomperts, R. E. Stratmann, O. Yazyev, A. J. Austin, R. Cammi, C. Pomelli, J. W. Ochterski, R. L. Martin, K. Morokuma, V. G. Zakrzewski, G. A. Voth, P. Salvador, J. J. Dannenberg, S. Dapprich, A. D. Daniels, . Farkas, J. F

Foresman, J. V. Ortiz, J. Cioslowski and D. J. Fox, *Gaussian 09 Revision D.01*, Gaussian Inc. Wallingford CT 2009.
43 N. M. O'Boyle, A. L. Tenderholt and K. M. Langner, *J. Comput. Chem.*, 2008, **29**, 839–845.
44 R. A. Marcus, *Rev. Mod. Phys.*, 1993, **65**, 599.
45 R. A. Marcus, *Annu. Rev. Phys. Chem.*, 1964, **15**, 155–196.
46 Y. A. Berlin, G. R. Hutchison, P. Rempala, M. A. Ratner and J. Michl, *J. Phys. Chem. A.*, 2003, **107**, 3970–3980.
47 B. S. Brunschwig, J. Logan, M. D. Newton and N. Sutin, *J. Am. Chem. Soc.*, 1980, **102**, 5798–5809.
48 J. E. Norton and J.-L. Brdas, *J. Am. Chem. Soc.*, 2008, **130**, 12377–12384.
49 I. Vilfan, *phys. status solidi (b)*, 1973, **59**, 351–360.
50 G. R. Hutchison, M. A. Ratner and T. J. Marks, *J. Am. Chem. Soc.*, 2005, **127**, 2339–2350.
51 H. Gao, C. Qin, H. Zhang, S. Wu, Z.-M. Su and Y. Wang, *J. Phys. Chem. A.*, 2008, **112**, 9097–9103.
52 T. Fujita, H. Nakai and H. Nakatsuji, *J. Chem. Phys.*, 1996, **104**, 2410–2417.
53 A. Troisi and G. Orlandi, *J. Phys. Chem. A.*, 2006, **110**, 4065–4070.
54 S. W. Yin, Y. P. Yi, Q. X. Li, G. Yu, Y. G. Liu and Z. G. Shuai, *J. Phys. Chem. A.*, 2006, **110**, 7138–7143.
55 B. M. Wong, M. Piacenza and F. D. Sala, *Phys. Chem. Chem. Phys.*, 2009, **11**, 4498–4508.
56 N. Martsinovich and A. Troisi, *Energy Environ. Sci.*, 2011, **4**, 4473–4495.
57 Y. Yi, L. Zhu and J.-L. Brdas, *J. Phys. Chem. C.*, 2012, **116**, 5215–5224.
58 L. J. Wang, G. J. Nan, X. D. Yang, Q. Peng, Q. K. Li and Z. G. Shuai, *Chem. Soc. Rev.*, 2010, **39**, 423–434.
59 J. Shi, L. Xu, Y. Li, M. Jia, Y. Kan and H. Wang, *Org. Electron.*, 2013, **14**, 934 – 941.
60 V. T. T. Huong, H. T. Nguyen, T. B. Tai and M. T. Nguyen, *J. Phys. Chem. C.*, 2013, **117**, 10175–10184.
61 P. v. R. Schleyer, M. Manoharan, Z.-X. Wang, H. Kiran, B.; Jiao, R. Puchta and N. J. R. v. E. Hommes, *Org. Lett.*, 2001, **3**, 2465–2468.
62 T. M. Krygowski, *J. Chem. Inf. Comput. Sci.*, 1993, **33**, 70–78.
63 M.-Y. Kuo, H.-Y. Chen and I. Chao, *Chem. Eur. J.*, 2007, **13**, 4750–4758.
64 L. Wang and H. Zhang, *J. Phys. Chem. C.*, 2011, **115**, 20674–20681.
65 L. Wang, G. Duan, Y. Ji and H. Zhang, *J. Phys. Chem. C.*, 2012, **116**, 22679–22686.
66 J.-D. Huang, S.-H. Wen, W.-Q. Deng and K.-L. Han, *J. Phys. Chem. B.*, 2011, **115**, 2140–2147.
67 V. I. Minkin, M. N. Glukhovtsev and B. Y. Simkin, *Aromaticity and Antiaromaticity*, Wiley, New York, 1994.
68 T. M. Krygowski, H. Szatylowicz, O. A. Stasyuk, J. Dominikowska and M. Palusiak, *Chem. Rev.*, 2014, **114**, 6383–6422.
69 W. B. Chen, H. X. Li, J. R. Widawsky, C. Appayee, L. Venkataraman and R. Breslow, *J. Am. Chem. Soc.*, 2014, **136**, 918–920.
70 M. L. Tang, J. H. Oh, A. D. Reichardt and Z. Bao, *J. Am. Chem. Soc.*, 2009, **131**, 3733–3740.
71 J. L. Brdas, J. P. Calbert, D. A. da Silva Filho and J. Cornil, *Proc. Natl. Acad. Sci.*, 2002, **99**, 5804–5809.
72 C. Kim, A. Facchetti and T. Marks, *Adv. Mater.*, 2007, **19**, 2561–2566.
73 L. Zhang, L. Tan, Z. H. Wang, W. P. Hu and D. B. Zhu, *Chem. Mater.*, 2009, **21**, 1993–1999.